Journal of Power Sources 250 (2014) 279–285

Contents lists available at ScienceDirect

Journal of Power Sources

journal homepage: www.elsevier.com/locate/jpowsour

Synthesis and characterization of carbon incorporated Fe–N/carbons for methanol-tolerant oxygen reduction reaction of polymer electrolyte fuel cells

Shou-Heng Liu [a,*], Jyun-Ren Wu [a], Chun-Jern Pan [b], Bing-Joe Hwang [b]

[a] Department of Chemical and Materials Engineering, National Kaohsiung University of Applied Sciences, Kaohsiung 80778, Taiwan
[b] Department of Chemical Engineering, National Taiwan University of Science and Technology, Taipei 10617, Taiwan

HIGHLIGHTS

- Carbon incorporated non-noble FeN_x catalysts were prepared via a facile route.
- ORR activity of the FeNC/C-3.1 catalysts was superior among the catalysts.
- The higher surface atomic N/C, Fe/C, and Fe–N_4 centers result in this enhancement.

ARTICLE INFO

Article history:
Received 20 September 2013
Received in revised form
4 November 2013
Accepted 9 November 2013
Available online 19 November 2013

Keywords:
Non-noble
N-doped
Carbide
Oxygen reduction reaction
X-ray absorption spectroscopy

ABSTRACT

A simple method has been developed for synthesis of carbons incorporating FeN_x electrocatalysts (FeNC/C-*z*) based on heat treatment of nitrogen-rich species (pentaethylenehexamine) and iron precursors ($FeCl_3$) on carbon blacks (Vulcan XC-72) under high temperature in a nitrogen atmosphere. These resulting catalysts have been fully characterized by various spectroscopic and analytical techniques such as X-ray diffraction (XRD), X-ray photoelectron spectroscopy (XPS) and X-ray absorption spectroscopy (XAS). Results obtained from the polarization curves show that FeNC/C-3.1 possesses the surpassing electrocatalytic activity and the tolerance to methanol crossover during the oxygen reduction reaction (ORR) among all the FeNC/C-*z* catalysts, which may be due to their higher surface Fe/C and N/C atomic ratios as well as a dominant carbon incorporated FeN_x ($x \approx 4$), as revealed from XPS and XAS spectroscopies.

1. Introduction

Fuel cells, in particular for direct methanol fuel cells (DMFCs) and proton-exchange membrane fuel cells (PEMFCs), have been recognized as one of the potential power sources for stationary and mobile applications. However, two major challenges, namely their costs and durability [1–5], limit the future large-scale commercialization applications of DMFCs/PEMFCs. In general, Pt-based catalysts have been intensively investigated because they are the most active and efficient electrocatalysts for oxygen reduction reaction (ORR) which is a sluggish and complicated four-electron reaction. Thus, it is crucial to develop alternative catalysts which possess reduced amounts of Pt [6–12] and even are Pt-free [13–19], meanwhile, increase their durability during long-term operation. In the recent reports, pyrolyzed transition metal together with nitrogen containing compounds in an inert or N-rich atmosphere, such as Fe based ethylenediamine, phthalocyanines, porphyrins, phenanthroline and tripyridyl triazine, etc. [20–26], has been extensively investigated and shown promising catalytic activity. However, the catalytic performance of aforementioned electrocatalysts is still incomparable to Pt based catalysts. Consequently, a more active non-noble electrocatalyst is extremely desirable to realize the cost-effective and industrial applications. Most recently, in order to enhance ORR performance, incorporation of carbons into iron nitride [21,27,28] or PdFe alloy [29] has been proposed, which may be a prospective method to create newly and effectively active sites for development of fuel cells.

The key scientific issues relating to the chemical forms of catalysts ultimately depend on their molecular-scale structures. Basic studies at this scale are necessary in the newly fabricated materials that may also facilitate the development of valuable tools for designing efficiency of devices. X-ray absorption near-edge

* Corresponding author. Tel.: +886 7 381 4526x5152; fax: +886 7 3830674.
E-mail address: shliu@kuas.edu.tw (S.-H. Liu).

0378-7753/$ – see front matter © 2013 Elsevier B.V. All rights reserved.
http://dx.doi.org/10.1016/j.jpowsour.2013.11.011

structural (XANES) spectroscopy can provide data regarding oxidation states of an excited atom, the coordination geometry, and the bonding of its local environment in catalysts, which can offer a helpful method to understand the superior properties of specific materials. Extended X-ray absorption fine structural (EXAFS) spectroscopy is a short-range structural probe which can supply speciation data such as bond distance, coordination number (CN) and local structures of crystalline and non-crystalline in the complex matrix. In the previous EXAFS studies, the nature of active sites and alloyed extents of target metal in the well-alloyed PtM [9,30–33] and PtRu [34–36] bifunctional electrocatalysts were examined during ORR and methanol oxidation, respectively. It should be noted that these EXAFS data are very useful in revealing the relationship between speciations of catalysts and their corresponding effects on catalytic reactions.

In this work, a facile route is reported to synthesize a series of carbon incorporated FeN_x (hereafter denoted as FeNC/C-*z*, where *z* represents the Fe content in wt%) by pyrolyzing different amounts of Fe(III) and pentaethylenehexamine (PEHA) on Vulcan XC-72 carbon blacks under high temperature in a nitrogen atmosphere. It is worthy to note that we adopt a nitrogen-rich compound (PEHA) which is cheap and simple ligand as a starting material for the first time to alternate porphyrins and phthalocyanines to synthesize non-precious metal ORR catalysts. The resultant FeNC/C-*z* electrocatalysts were coated onto a glassy carbon electrode for electrochemical ORR measurements by using cyclic voltammetry (CV), linear sweep voltammetry (LSV) and rotating disk electrode (RDE) techniques. Moreover, the probably structural information of novel FeNC/C-*z* catalysts was further explored by X-ray based spectroscopies, such as X-ray diffraction (XRD), X-ray photoelectron spectroscopy (XPS) and X-ray absorption spectroscopy (XAS). The prepared FeNC/C-*z* catalysts possess not only surpassing activity but also tolerance to methanol crossover favorable for ORR and thus may render cost-effective and practical applications as cathodic electrocatalysts for DMFCs and PEMFCs.

2. Experimental

2.1. Catalysts preparation

To fabricate carbon incorporated FeN_x samples, a simple route has been proposed as below. Firstly, for the preparation of a Fe–PEHA complex solution, the mole ratio of PEHA/Fe was maintained constant at 2. In a typical synthesis, weighted amounts of the iron (III) chloride ($Fe(III)Cl_3$, Acros) were dissolved in 3% ethanol solution, followed by slowly adding pentaethylenehexamine (PEHA, Acros) to form dark red FeN_x chelates solution. Then, carbon blacks (Vulcan XC-72, Cabot Corp.) were added under stirring for 48 h. The solvents were eliminated by using a vacuum oven at 363 K. Finally, the resulting powders were ramped to 1073 K with a heating rate of 5 K min^{-1} and kept at the same temperature for 2 h under nitrogen atmosphere. To remove excess Fe metals on the surface of the catalyst, the heat-treated sample was leached in 0.5 M H_2SO_4 at 353 K for ca. 8 h. The obtained samples were denoted as FeNC/C-*z* (where *z* represents the Fe content in wt%).

2.2. Characterization methods

The amounts of iron in the FeNC/C-*z* samples were measured by atomic absorption spectroscopy (AAS, ICE-3300). To obtain bulk compositions of samples, elemental analyses (EA) were performed by using a CHN elemental analyzer (Heraeus varioIII). X-ray diffraction (XRD) patterns were acquired using a PANalytical (X'Pert PRO) diffractometer equipped with CuKα as a radiation source ($\lambda = 0.1541$ nm). Surface compositions of samples were estimated by using X-ray photoelectron spectroscopy (XPS) which was obtained on a spectrometer (Kratos Axis Ultra DLD) with a constant pass energy of 20 eV and a monochromatic Al-Ka X-ray (1486.6 eV) under ultra-high vacuum condition (10^{-10} Torr). The Fe K-edge X-ray absorption spectroscopy (XAS) of the samples was performed using a transmission mode at the Wiggler beamlines 17C of the National Synchrotron Radiation Research Center (NSRRC) in Taiwan. A Si(111) double-crystal monochromator was used for detuning energy with a resolution of 2×10^{-4}. Two ionization chambers filled with mixture gases were used in series to measure the intensities of the incident beam (I_o) and the beam transmitted through the sample (I_t). A third ion chamber was used in conjunction with a reference sample (Fe K-edge measurements). For XAS data analysis, each EXAFS function (χ) was obtained by subtracting the post-edge background from the overall absorption, followed by normalizing with respect to the edge jump step. Afterward, k^3-weighted $\chi(k)$ spectra in the *k*-space, ranging from 3.5 to 12.0 $Å^{-1}$ were Fourier transformed to the *r*-space to separate the EXAFS contributions from different coordination shells. A nonlinear least-squares algorithm was utilized to fit the EXAFS spectra without phase correction in the *r*-space between 0.9 and 3.0 Å. The backscattering amplitude and the phase shift for the specific atom pairs were theoretically calculated using the FEFF7 code [37]. The data in the EXAFS analyses were done by using the Athena and Artemis software [38].

2.3. Electrocatalytic properties measurements

A single compartment glass cell with a conventional three-electrode configuration was used to measure electrocatalytic properties of FeNC/C-*z*. A glassy carbon (GC) electrode (5 mm in diameter) was utilized as a working electrode and a saturated Ag/AgCl electrode and a platinum wire were used as reference and counter electrodes, respectively. All electrochemical results reported in this work referred to the reversible hydrogen electrode (RHE). To prepare GC thin-film electrode, the surface of GC electrode was firstly polished with alumina powder. Subsequently, ca. 5 mg of sample was added into 2.5 mL deionized water, followed by ultrasonic treatment for 0.5 h. Then, ca. 20 μL of the resultant suspension mixture was placed onto the GC electrode, followed by drying in air at 333 K for 1 h. Finally, 20 μL of 5% Nafion® (DuPont) solution was covered on the catalyst layer to make sure good adhesion of the catalyst onto the GC electrode. Electrocatalytic activity measurements of FeNC/C-*z* were carried out on a potentiostat/galvanostat (CHI Instruments, 727D) equipped with a rotating disk electrode (RDE) system (Pine Instrument, AFMSRCE). Cyclic voltammetry (CV) experiments were performed between 0 and 1.2 V in a 0.5 M H_2SO_4 solution under high-purity N_2 (99.9%) to clean and activate the electrode surface until the stable CV curves were obtained. ORR polarization curves of all FeNC/C-*z* were obtained by using a linear sweep voltammetry (LSV) technique which an RDE system (rotating speed of 1600 rpm) was applied to scan the potential range from 0.1 to 1.0 V vs. RHE with the scan rate of 5 mV s^{-1} under oxygen saturated 0.5 M H_2SO_4 electrolyte.

3. Results and discussion

XRD patterns of all the FeNC/C-*z* are shown in Fig. 1. The intensities and position of the diffraction lines for Fe, Fe_2N and Fe_3C are also included in the bottom of Fig. 1. It can be seen that a broad diffraction peak located at ca. 24.6° which is related to the (002) plane reflection feature of graphitic carbon. No apparent diffraction features were observed due to the small loading of Fe (3.1 wt%) onto carbon supports and pyrolyzing at 1073 K. Upon the amounts of the Fe loading are further increased to 8.2 wt%, a main diffraction peak

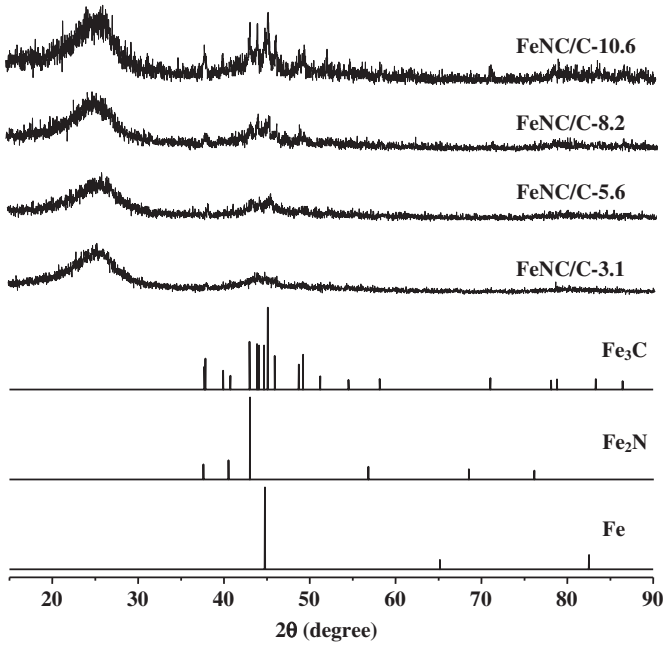

Fig. 1. XRD patterns of various FeNC/C-*z* samples.

centered at 2θ = ca. 44.8° suggests the possible existence of the crystalline planes of metallic α-Fe (JCPDS, No. 87-0722). The remaining of diffraction peaks may be attributed to characteristics of Fe_3C (JCPDS, No. 89-2867) and Fe_2N phases (JCPDS, No. 89-3939). As a result, XRD patterns indicate that the FeNC/C-*z* samples may be composed of a mixture of Fe_3C, Fe_2N and metallic Fe phases. It should be noted that chemical structures of Fe are unable to obviously differentiate because the features of Fe_3C, Fe_2N and α-Fe are to some extent overlaid in the XRD patterns. Moreover, some Fe species could be scarcely detected by using XRD due to the presence of amorphous phase. Accordingly, additional XPS and XAS analyses were employed to further investigate information including chemical environment of nitrogen, the coordination geometry, and the bonding of its local environment around the Fe atoms.

The surface compositions of FeNC/C-*z* catalysts were examined by using XPS. Fig. S1 (see Supplementary Material) shows the XPS survey spectra at C 1s, N 1s, O 1s and Fe 2p3 regions and their corresponding surface atomic compositions (at.%) are also included in Table 1. Among all the FeNC/C-*z* catalysts, we found that FeNC/C-3.1 exhibits a higher surface atomic nitrogen content (3.0 at.%) which is higher than the bulk nitrogen content (2.8%) measured by EA, indicating that nitrogen atoms are doped mostly on the surface of FeNC/C-3.1 catalysts. In addition, the FeNC/C-3.1 has the highest surface atomic ratio of N/C (3.7%) in the FeNC/C-*z* catalysts.

Table 1
Physical properties of various FeNC/C-*z* samples.

Sample	Fe[a] (%)	N[b] (%)	Fe[c] (at.%)	C[c] (at.%)	N[c] (at.%)	O[c] (at.%)	N/C[d] (%)	Fe/C[d] (%)
FeNC/C-3.1	3.1	2.8	2.2	81.8	3.0	13.0	3.7	2.7
FeNC/C-5.6	5.6	2.8	1.7	85.1	2.0	11.3	2.3	2.0
FeNC/C-8.2	8.2	2.1	1.7	82.5	2.1	13.7	2.5	2.1
FeNC/C-10.6	10.6	2.3	2.3	82.8	2.0	12.9	2.4	2.7

[a] Fe content (wt%) analyzed by AAS.
[b] Determined by EA.
[c] Obtained from XPS analysis.
[d] Atomic ratio calculated from the table.

According to previous reports [24], the higher nitrogen content doped onto the catalysts surface would lead to the better ORR performance. The structural features of these N species on the surfaces of various FeNC/C-*z* (z = 3.1, 8.2, 10.6) samples were further analyzed by high-resolution XPS studies, as shown in Fig. 2. At N 1s region, all the samples typically reveal three overlapped peaks centered at ca. 398.5, 400.8 and ≥403.5 eV. The first peak at 398.5 eV can be attributed to the presence of pyridinic-N species [39], by which each N atom is bonded with two carbon atoms locating on the edges of graphite planes. As such, these pyridinic-N species are inclined to donate a p electron to the aromatic π-system. The second peak at ca. 400.8 eV can be ascribed to quaternary-N species [39], by which each N atom is connected with three carbon atoms within a graphite plane, thus, they are also known as the 'graphitic nitrogen' species. Whereas, the weaker peak centered at ≥403.5 eV may be assigned to pyridinic-N^+-O^- species which their assignment and corresponding contribution to catalytic performance is unclear [24]. Further spectral analyses by Gaussian deconvolution enable us to evaluate the relative quaternary- vs. pyridinic-N concentrations on the surfaces of various FeNC/C-*z* samples, as listed in Table 2. For FeNC/C-*z* samples with z = 3.1, 8.2, 10.6, a progressive increase in pyridinic-N content with decreasing Fe loading can be observed. According to the recent

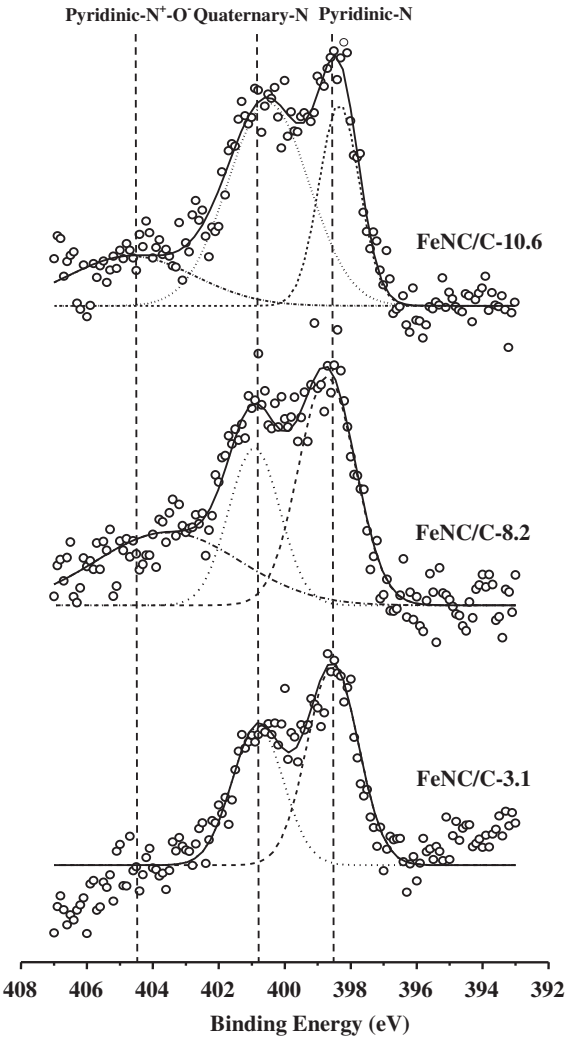

Fig. 2. XPS spectra of FeNC/C-3.1, FeNC/C-8.2 and FeNC/C-10.6 catalysts at the N 1s region.

Table 2
The assignments, binding energies, and concentrations of N 1s species in various FeNC/C-*z* samples obtained from XPS results.

Sample	Assignment	B.E. (eV)	Concentration (%)
FeNC/C-3.1	Pyridinic-N	398.5	58.8
	Quaternary-N	400.8	41.2
FeNC/C-8.2	Pyridinic-N	398.7	41.1
	Quaternary-N	400.9	25.4
	Pyridinic-N^+-O^-	403.5	33.5
FeNC/C-10.6	Pyridinic-N	398.3	26.3
	Quaternary-N	400.5	53.4
	Pyridinic-N^+-O^-	404.6	20.3

studies [40–42], quaternary-N (graphitic nitrogen) is reported to be more important for the electrocatalytic activities of nitrogen-doped carbons during ORR. In some studies, the enhancement of ORR with a four electron mechanism is attributed to the pyrrolic-N and the pyridinic-N is not able to facilitate direct four electron pathways for ORR without the assistance of pyrrolic-N and/or quaternary-N [43,44]. Nonetheless, since pyridinic-N species in this work are recognized as the most active sites for coordination of metal ions [45–47], an increase in its concentration (58.8%), which is also associated with an increase in the total nitrogen content (3.0%) in the FeNC/C-3.1 samples, should be responsible for the observed increase in ORR activity as discussed below.

In order to further realize electronic states and atomic bonding environment of iron in FeNC/C-*z* during ORR, X-ray absorption spectroscopies were also obtained using a synchrotron radiation light source. Generally, XANES can be employed to study the excitation of a core electron to quasi-bound states. Thus, the corresponding positions of the edge in the samples are related to the valence of the central atom [48]. The normalized K-edge XANES spectra of FeNC/C-*z* (z = 3.1, 8.2, 10.6) electrocatalysts and model compounds (Fe foil, Fe_2O_3 and $FeCl_3$) are shown in Fig. 3. The shapes of the FeNC/C-*z* in the XANES regions are totally different from that of the $FeCl_3$ model compound, indicating that the iron precursors were transformed to other form of iron during high-temperature pyrolysis process. The absorption edge at 7130 eV is attributed to 1s to 4p electronic transition of iron metal. In general, their corresponding magnitude of the absorption hump is defined as white line. As we can see in Fig. 3, the white line intensities of FeNC/C-*z* are between those of iron metal and iron(III) oxide (Fe_2O_3). Moreover, the pre-edge curves of the FeNC/C-*z* are located between those of iron metal and iron(III) oxide (Fe_2O_3), suggesting the local electronic states and the existence of oxidative valence of iron in the FeNC/C-*z*. It is noteworthy that FeNC/C-3.1 possesses the largest valence among all the FeNC/C-*z* electrocatalysts. Fourier Transformations (FT) of the EXAFS oscillations $k^3\chi(k)$ obtained for FeNC/C-*z* electrocatalysts and iron model compounds are compared and shown in Fig. 4. It can be clearly seen that the local structures of FeNC/C-*z* are notably different from those of model compounds ($FeCl_3$, Fe_2O_3 and Fe foil). The main peaks observed for FeNC/C-*z* electrocatalysts in the FT spectra at ca. 1.5 Å are due to the first shell iron bonded to nitrogen and carbon atoms, which verify the probable formation of FeN_xC_y clusters. The other features located at 2.1 Å corresponding to the scattering from iron atoms in the second coordination shells. Based on a model using Fe–N, Fe–C, and Fe–Fe paths to differentiate the short-range structure around the iron atoms, EXAFS parameters such as the coordination number (CN), bond distance (R), Debye–Waller factor (σ^2), and inner potential shift (ΔE) were obtained by curve fitting analyses, as summarized in Table 3. The FeNC/C-3.1 electrocatalysts have Fe–N (2.03 Å), Fe–C (2.17 Å) and Fe–Fe (2.70 Å) bonding with CNs of 4.1, 14.1, 1.8, respectively. This finding again indicates that FeN_xC_y clusters

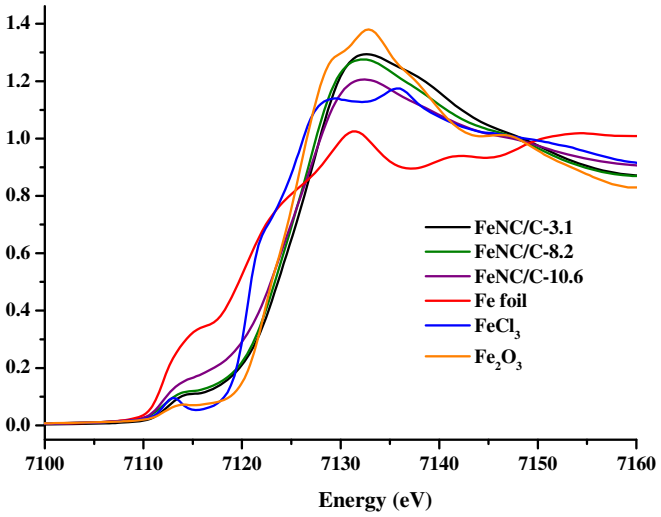

Fig. 3. Fe K-edge XANES spectra of model compounds and FeNC/C-*z* samples.

[27,28,49] may be simultaneously produced during high-temperature heat treatment in which the sintering reaction between metallic iron may be limited because of the presence of carbon blacks (Vulcan XC-72). Thus, the formation of FeN_xC_y clusters is observed due to the enhanced diffusion of carbon atoms into the lattice of FeN_x moieties, as evidenced by the noticeable coordination numbers of carbon binding to iron. It has been reported that iron metals can be incorporated onto carbon supports to produce iron carbide species through an anchoring interaction [50]. In the case of heat treatment under high temperature, the probability of binding between iron and carbon atoms may be

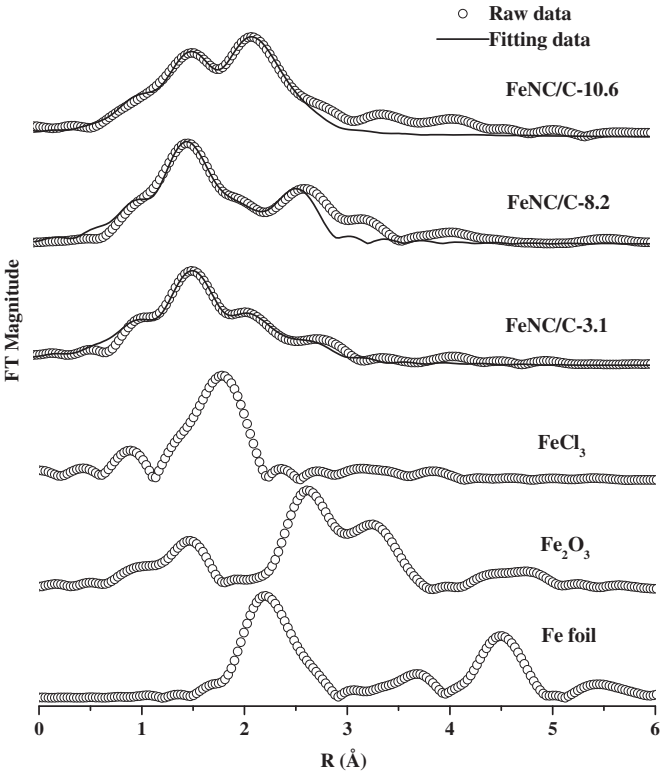

Fig. 4. Curve-fitting Fourier transform of k^3-weighted $\chi(k)$ Fe K-edge EXAFS spectrum for FeNC/C-*z* samples and Fe model compounds.

Table 3
EXAFS structural parameters derived from fitting results at Fe K-edge for the FeNC/C-*z* samples.

Sample	Shell	CN[a]	*R* (Å)[b]	$\sigma^2 \times 10^{-3}$ (Å^2)[c]	Δ*E* (eV)[d]
FeNC/C-3.1	Fe–N	4.1(±0.4)	2.03(±0.02)	9.8	10.3
	Fe–C	14.1(±1.2)	2.17(±0.03)	16.3	−7.7
	Fe–Fe	1.8(±0.4)	2.70(±0.05)	20.9	10.2
FeNC/C-8.2	Fe–N	1.2(±0.1)	1.98(±0.01)	2.7	9.0
	Fe–C	7.3(±0.8)	2.13(±0.02)	12.2	−4.9
	Fe–Fe	1.0(±0.2)	2.74(±0.03)	9.2	10.9
FeNC/C-10.6	Fe–N	5.2(±0.5)	2.03(±0.02)	9.0	6.9
	Fe–C	10.7(±1.0)	2.19(±0.02)	11.6	−9.3
	Fe–Fe	3.0(±0.8)	2.66(±0.04)	15.2	3.9

[a] CN: Coordination number.
[b] *R*: Bond distance.
[c] σ^2: Debye–Waller factor.
[d] Δ*E*: Inner potential shift.

increased. However, the aggregation of iron metals would happen (CN of Fe–Fe = 3.0) while the content of iron metals is increased to 10.6%. As mentioned later, these distinctive active centers of Fe–N–C in the FeNC/C-3.1 electrocatalysts may be accountable for the superior ORR performance among all the catalysts.

The electrocatalytic performance of FeNC/C-*z* catalysts during ORR was investigated by linear sweep voltammetry (LSV) tests, which were carried out in oxygen saturated 0.5 M H_2SO_4 solution at room temperature. For comparison, the polarization curve of FeNC/C-*z* and a commercially available JM-Pt/C (Johnson-Matthey; 20 wt % Pt on Vulcan XC-72 activated carbon) are shown in Fig. 5 and also summarized in Table 4. An onset potential of ca. 0.77 V was observed for the FeNC/C-10.6 catalyst. Upon the decreased loading of iron, the increases in onset potential were observed. Consequently, the FeNC/C-3.1 was found to have the best ORR electrocatalytic performance (onset potential = 0.83 V) among all the FeNC/C-*z* catalysts. Additionally, the ORR mass activity of FeNC/C-3.1 at 0.7 V reaches ca. 1.2 mA $mg^{-1}_{catalyst}$ which is higher than the value reported in the literature [51]. Moreover, the ORR activity of FeNC/C-3.1 is around 67% of that of commercial JM-Pt/C at 0.5 V. To further explore ORR mechanism quantitatively, the number of electrons (*n*) involved during ORR in the FeNC/C-*z* electrocatalysts was evaluated by Koutecky–Levich equation [52,53]. The RDE experiments of the FeNC/C-*z* electrocatalysts were conducted in O_2 saturated 0.5 M H_2SO_4 solution at room temperature under different rotating rates and their corresponding Koutecky–Levich plots at 0.3 V vs. RHE are shown in Fig. 6. For comparison, the theoretical plots of the two-electron and four-electron transfer processes during ORR are also shown in Fig. 6. Based on the Koutecky–Levich first-order reaction equation, *n* values can be derived from the slope as the reciprocal diffusion-limiting current density (i^{-1}) is plotted as a function vs. the reciprocal rotating angular frequency ($\omega^{-1/2}$). Accordingly, *n* values of FeNC/C-*z* electrocatalysts with *x* = 3.1, 5.6, 8.2 and 10.6 were deduced to be 3.1, 2.1, 2.5 and 1.9

Table 4
Kinetic parameters of various FeNC/C-*z* electrocatalysts during ORR.

Sample	E_{onset}[a] (V)	j_{mass}[b] (mA $mg^{-1}_{catalyst}$)	*n*
FeNC/C-3.1	0.83	1.2	3.1
FeNC/C-5.6	0.80	1.0	2.1
FeNC/C-8.2	0.78	0.5	2.5
FeNC/C-10.6	0.77	0.4	1.9

[a] Onset potential vs. RHE.
[b] Kinetic mass current densities at 0.7 V vs. RHE.

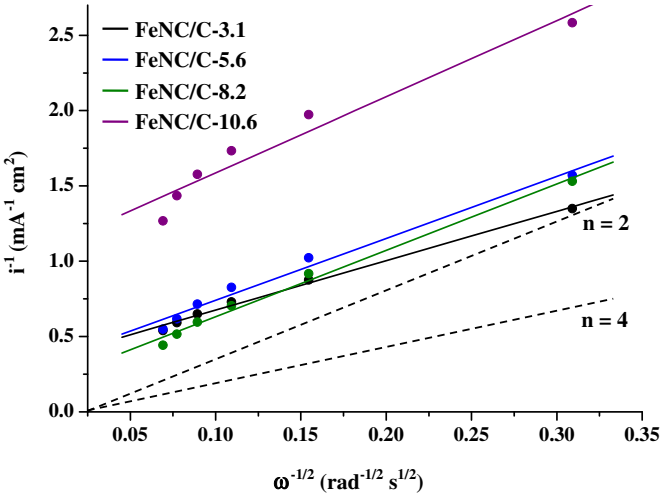

Fig. 6. Koutecky–Levich plots during ORR for various FeNC/C-*z* catalysts at 0.3 V vs. RHE in O_2 saturated 0.5 M H_2SO_4 solution at room temperature.

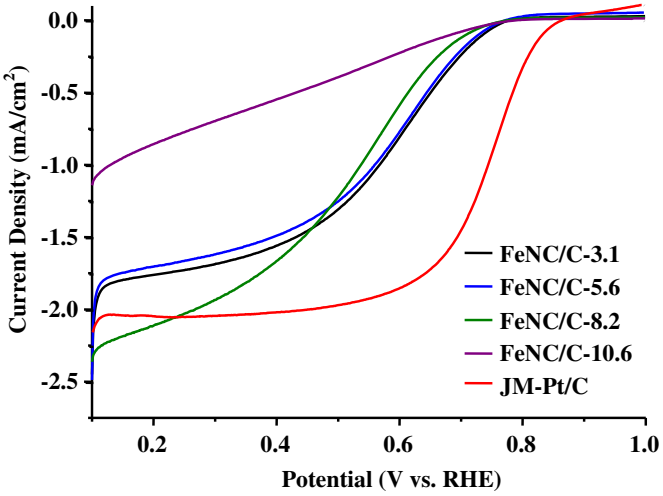

Fig. 5. Polarization curves during oxygen reduction for various FeNC/C-*z* and commercial JM-Pt/C catalysts in O_2 saturated 0.5 M H_2SO_4 solution at room temperature.

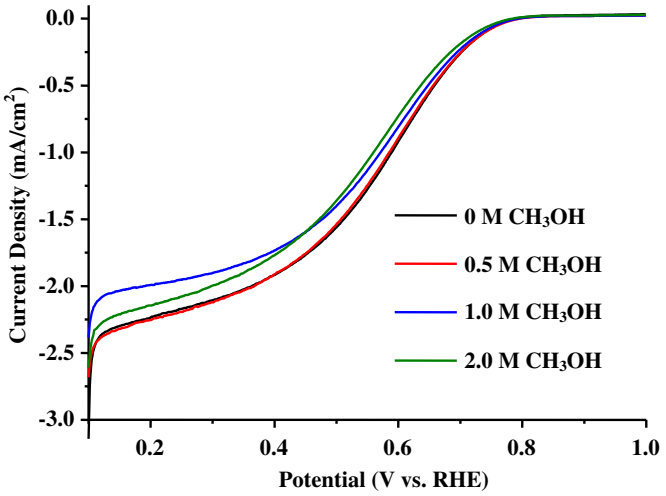

Fig. 7. Polarization curves for ORR on FeNC/C-3.1 with various concentrations of CH_3OH in O_2 saturated 0.5 M H_2SO_4 solution.

(see Table 4), respectively, implying that FeNC/C-3.1 electrocatalysts are dominantly proceeded ORR with four-electron transferred pathway. Unlike two-electron reduction reactions for FeNC/C-z (z = 5.6, 8.2 and 10.6), FeNC/C-3.1 electrocatalysts can circumvent the production of hydrogen peroxide radicals which lead to an undesirable degradation of the membrane-electrolyte-assembly (MEA) of the fuel cells. Based on the XPS data in Table 1, it can be observed that the N/C and Fe/C atomic ratios of FeNC/C-3.1 are the highest among the FeNC/C-z. The high N/C and Fe/C atomic ratios, and the moderate FeN_x coordination number ($x \approx 4$, in Table 3) which were characterized by XPS and EXAFS show that the surface iron concentration and the number of iron coordinated with proper pyridinic-N should be responsible for the superior ORR performance of FeNC/C-3.1.

The electrocatalytic durability and tolerance to the methanol crossover at the cathode have been considered as two of the most critical issues for fuel cells [54–56]. To further study the methanol-tolerant properties of the synthesized FeNC/C-z electrocatalysts, a series of LSV tests were also performed to reveal the effect of different concentrations of methanol (0.5–2 M) on electrocatalytic ORR performance of FeNC/C-3.1 catalysts. As shown in Fig. 7, little increase in overpotential is observed for FeNC/C-3.1 electrocatalysts even in the presence of 2 M methanol as compared to ORR in pure H_2SO_4 solution. The significant inhibition in ORR overpotential on the FeNC/C-3.1 catalysts is due to the weak competition reaction between oxygen reduction and methanol oxidation, which could be attributed to the unique properties of carbon-incorporated FeN_x catalysts ($x \approx 4$). Transition metal N_4 chelates [57,58] were reported to have highly methanol-tolerant ability during ORR.

4. Conclusions

In summary, we report a facile method to prepare carbons incorporated FeN_x electrocatalysts (FeNC/C-z) with various Fe loadings in this study. Electrocatalytic ORR polarization curves were used to evaluate their corresponding activities. Among all the FeNC/C-z electrocatalysts, FeNC/C-3.1 was found to have the superior ORR properties. In addition, transferred electron number obtained from Koutecky–Levich equation suggests that the FeNC/C-3.1 is mostly four-electron transferred ORR process. From XPS data, the FeNC/C-3.1 was also found to possess the notable increases in the atomic surface Fe/C and N/C ratios and more pyridinic-N sites. Moreover, combining the results from XRD and XAS spectroscopies, it can be observed that carbons may incorporate into the FeN_4 matrix to form Fe–N–C active centers which are attributed to the significant ORR enhancement with methanol tolerance. Thus, these FeNC/C-3.1 nanocomposites may render future cost-effective applications in hydrogen-energy related areas, for instance, as electrocatalysts for PEMFCs and DMFCs.

Acknowledgments

Financial support of this work from the National Science Council, Taiwan (Contract No.: NSC99-2221-E-151-044-MY2) is gratefully acknowledged.

Appendix A. Supplementary material

Supplementary data related to this article can be found at http://dx.doi.org/10.1016/j.jpowsour.2013.11.011.

References

[1] Y.Y. Shao, G.P. Yin, Y.Z. Gao, J. Power Sources 171 (2007) 558–566.
[2] G. Gupta, D.A. Slanac, P. Kumar, J.D. Wiggins-Camacho, J. Kim, R. Ryoo, K.J. Stevenson, K.P. Johnston, J. Phys. Chem. C 114 (2010) 10796–10805.
[3] S.-H. Liu, C.-C. Chiang, M.-T. Wu, S.-B. Liu, Int. J. Hydrogen Energy 35 (2010) 8149–8154.
[4] S.-H. Liu, S.-C. Chen, W.-H. Sie, Int. J. Hydrogen Energy 36 (2011) 15060–15067.
[5] D.Z. Mezalira, M. Bron, J. Power Sources 231 (2013) 113–121.
[6] E. Billy, F. Maillard, A. Morin, L. Guetaz, F. Emieux, C. Thurier, P. Doppelt, S. Donet, S. Mailley, J. Power Sources 195 (2010) 2737–2746.
[7] C.S. Rao, D.M. Singh, R. Sekhar, J. Rangarajan, Int. J. Hydrogen Energy 36 (2011) 14805–14814.
[8] J. Zhao, A. Manthiram, Appl. Catal. B: Environ. 101 (2011) 660–668.
[9] S.-H. Liu, F.S. Zheng, J.-R. Wu, Appl. Catal. B: Environ. 108–109 (2011) 81–89.
[10] F. Su, C.K. Poh, J.H. Zeng, Z.Y. Zhong, Z.L. Liu, J.Y. Lin, J. Power Sources 205 (2012) 136–144.
[11] K. Jayasayee, J.A.R. Van Veen, T.G. Manivasagam, S. Celebi, E.J.M. Hensen, F.A. de Bruijn, Appl. Catal. B: Environ. 111 (2012) 515–526.
[12] Z. Yang, H.G. Nie, X. Chen, X.H. Chen, S.M. Huang, J. Power Sources 236 (2013) 238–249.
[13] L. Zhang, J.J. Zhang, D.P. Wilkinson, H.J. Wang, J. Power Sources 156 (2006) 171–182.
[14] H.J. Zhang, Q.Z. Jiang, L. Sun, X.X. Yuan, Z. Shao, Z.F. Ma, Int. J. Hydrogen Energy 35 (2010) 8295–8302.
[15] G. Wu, K.L. More, C.M. Johnston, P. Zelenay, Science 332 (2011) 443–447.
[16] T. Palaniselvam, R. Kannan, S. Kurungot, Chem. Commun. 47 (2011) 2910–2912.
[17] Z.W. Chen, D. Higgins, A. Yu, L. Zhang, J. Zhang, Energy Environ. Sci. 4 (2011) 3167–3192.
[18] R. Liu, C. von Malotki, L. Arnold, N. Koshino, H. Higashimura, M. Baumgarten, K. Müllen, J. Am. Chem. Soc. 133 (2011) 10372–10375.
[19] S.H. Lim, Z.T. Li, C.K. Poh, L.F. Lai, J.Y. Lin, J. Power Sources 214 (2012) 15–20.
[20] G. Lalande, G. Faubert, R. Cote, D. Guay, J.P. Dodelet, L.T. Weng, P. Bertrand, J. Power Sources 61 (1996) 227–237.
[21] F. Charreteur, F. Jaouen, J.P. Dodelet, Electrochim. Acta 54 (2009) 6622–6630.
[22] G. Liu, X. Li, P. Ganesan, B.N. Popov, Appl. Catal. B: Environ. 93 (2009) 156–165.
[23] L. Zhang, K. Lee, C.W.B. Bezerra, J.L. Zhang, J.J. Zhang, Electrochim. Acta 54 (2009) 6631–6636.
[24] J.Y. Choi, R.S. Hsu, Z.W. Chen, J. Phys. Chem. C 114 (2010) 8048–8053.
[25] J.T. Wang, S. Li, G.W. Zhu, W. Zhao, R.X. Chen, M. Pan, J. Power Sources 240 (2013) 381–389.
[26] F.J. Pérez-Alonso, M. Abdel Salam, T. Herranz, J.L. Gómez de la Fuente, S.A. Al-Thabaiti, S.N. Basahel, M.A. Peña, J.L.G. Fierro, S. Rojas, J. Power Sources 240 (2013) 494–502.
[27] C.-W. Tsai, H.M. Chen, R.-S. Liu, K. Asakura, L. Zhang, J. Zhang, M.-Y. Lo, Y.-M. Peng, Electrochim. Acta 56 (2011) 8734–8738.
[28] C.-W. Tsai, M.-H. Tu, C.-J. Chen, T.-H. Hung, R.-S. Liu, W.-R. Liu, M.-Y. Lo, Y.-M. Peng, L. Zhang, J. Zhang, D.-S. Shy, X.-K. Xing, RSC Adv. 1 (2011) 1349–1357.
[29] Y.-C. Yeh, H.M. Chen, R.-S. Liu, K. Asakura, M.-Y. Lo, Y.-M. Peng, T.-S. Chan, J.-F. Lee, Chem. Mater. 21 (2009) 4030–4036.
[30] F.H.B. Lima, J.F.R. de Castro, L.G.R.A. Santos, E.A. Ticianelli, J. Power Sources 190 (2009) 293–300.
[31] A.R. Malheiro, J. Perez, H.M. Villullas, J. Power Sources 195 (2010) 3111–3118.
[32] S.J. Hwang, S.J. Yoo, S. Jang, T.H. Lim, S.A. Hong, S.K. Kim, J. Phys. Chem. C 115 (2011) 2483–2488.
[33] N. Ishiguro, T. Saida, T. Uruga, S. Nagamatsu, O. Sekizawa, K. Nitta, T. Yamamoto, S. Ohkoshi, Y. Iwasawa, T. Yokoyama, M. Tada, ACS Catal. 2 (2012) 1319–1330.
[34] S.-H. Liu, W.-Y. Yu, C.-H. Chen, A.-Y. Lo, B.-J. Hwang, S.-H. Chien, S.-B. Liu, Chem. Mater. 20 (2008) 1622–1628.
[35] T.A. Yamamoto, S. Kageyama, S. Seino, H. Nitani, T. Nakagawa, R. Horioka, Y. Honda, K. Ueno, H. Daimon, Appl. Catal. A: Gen. 396 (2011) 68–75.
[36] C.-W. Kuo, I.-T. Lu, L.-C. Chang, Y.-C. Hsieh, Y.-C. Tseng, P.-W. Wu, J.-F. Lee, J. Power Sources 240 (2013) 122–130.
[37] S. Zabinsky, J.J. Rehr, A.L. Ankudinov, R.C. Albers, M. Eller, J. Phys. Rev. B 52 (1995) 2995–3009.
[38] B. Ravel, M. Newville, J. Synchrotoron Radiat. 12 (2005) 537–541.
[39] J.R. Pels, F. Kapteijn, J.A. Moulijn, Q. Zhu, K.M. Thomas, Carbon 33 (1995) 1641–1653.
[40] H. Niwa, K. Horiba, Y. Harada, M. Oshima, T. Ikeda, K. Terakura, J. Ozaki, S. Miyata, J. Power Sources 187 (2009) 93–97.
[41] Z.Y. Lin, G.H. Waller, Y. Liu, M.L. Liu, C.-P. Wong, Nano Energy 2 (2013) 241–248.
[42] M. Sevilla, L.H. Yu, T.P. Fellinger, A.B. Fuertes, M. Titirici, RSC Adv. 3 (2013) 9904–9910.
[43] Z. Luo, S. Lim, Z. Tian, J. Shang, L. Lai, B. MacDonald, C. Fu, Z. Shen, T. Yu, J. Lin, J. Mater. Chem. 21 (2011) 8038–8044.
[44] S.M. Unni, S. Devulapally, N. Karjule, S. Kurungot, J. Mater. Chem. 22 (2012) 23506–23513.
[45] P.H. Matter, L. Zhang, U.S. Ozkan, J. Catal. 239 (2006) 83–96.
[46] H.R. Byon, J. Suntivich, Y. Shao-Horn, Chem. Mater. 23 (2011) 3421–3428.
[47] U.I. Kramm, J. Herranz, N. Larouche, T.M. Arruda, M. Lefèvre, F. Jaouen, P. Bogdanoff, S. Fiechter, I. Abs-Wurmbach, S. Mukerjee, J.P. Dodelet, Phys. Chem. Chem. Phys. 14 (2012) 11673–11688.

[48] Y. Iwasawa, X-ray Absorption Fine Structure for Catalyst and Surfaces, World Scientific, Singapore, 1996.
[49] S.-H. Liu, J.-R. Wu, Micropor. Mesopor. Mater. 170 (2013) 150–154.
[50] N. Travitsky, T. Ripenbein, D. Golodnitsky, Y. Rosenberg, L. Burshtein, E. Peled, J. Power Sources 161 (2006) 782–789.
[51] C.H. Choi, S.Y. Lee, S.H. Park, S.I. Woo, Appl. Catal. B: Environ. 103 (2011) 362–368.
[52] S.-H. Liu, M.-T. Wu, Y.-H. Lai, C.-C. Chiang, N. Yu, S.-B. Liu, J. Chem. Mater. 21 (2011) 12489–12496.
[53] M. Ammam, E.B. Easton, J. Power Sources 236 (2013) 311–320.
[54] P. Hernández-Fernández, S. Rojas, P. Ocón, A. de Frutos, J.M. Figueroa, P. Terreros, M.A. Peña, J.L.G. Fierro, J. Power Sources 177 (2008) 9–16.
[55] S.-H. Liu, J.-R. Wu, Int. J. Hydrogen Energy 36 (2011) 87–93.
[56] Y.F. Tang, F.M. Gao, S.X. Yu, Z.P. Li, Y.F. Zhao, J. Power Sources 239 (2013) 374–381.
[57] A.L. Bouwkamp-Wijnoltz, W. Visser, J.A.R. Van Veen, Electrochim. Acta 43 (1998) 3141–3152.
[58] S. Baranton, C. Coutanceau, C. Roux, F. Hahn, J.-M. Léger, J. Electroanal. Chem. 577 (2005) 223–234.